Arsenate removal from aqueous solution using chitosan-coated bentonite, chitosan-coated kaolinite and chitosan-coated sand: parametric, isotherm and thermodynamic studies

Cybelle M. Futalan, Yu-Shen Huang, Jheng-Hong Chen and Meng-Wei Wan

ABSTRACT

In the present work, the removal efficiency of As(V) from aqueous solution using chitosan-coated bentonite (CCB), chitosan-coated kaolinite (CCK) and chitosan-coated sand (CCS) was evaluated. The chitosan-based adsorbents were characterized using scanning electron microscopy, Fourier-transform infrared spectroscopy, the Brunauer–Emmett–Teller method and thermogravimetric analysis. Kinetic studies revealed that As(V) uptake using CCB, CCK and CCS fitted well with the pseudo-second order equation ($R^2 \geq 0.9847$; $RMSE \leq 9.1833$). Equilibrium data show good correlation with the Langmuir model ($R^2 \geq 0.9753$; $RMSE \leq 8.5123$; $SSE \leq 16.2651$) for all adsorbents, which implies monolayer coverage onto homogenous energy sites. The Langmuir adsorption capacity for As (V) at pH 7.0 was determined to be 67.11, 64.85, and 16.78 mg/g for CCB, CCK and CCS, respectively. Thermodynamic studies show that As(V) uptake is exothermic in nature using CCK and endothermic using CCB and CCS. Moreover, adsorption of As(V) was feasible and spontaneous for CCB and CCS at 298 to 328 K. Results show that CCB is the most effective adsorbent in the removal of As(V) from water due to its high surface area and large pore diameter.

Key words | arsenate, bentonite, chitosan, kaolinite, sand, thermodynamics

Cybelle M. Futalan
National Research Center for Disaster-Free and Safe Ocean City,
Busan 49315,
Republic of Korea

Yu-Shen Huang
Department of Environmental Engineering and Science,
Chia-Nan University of Pharmacy and Science,
Tainan 71710,
Taiwan

Jheng-Hong Chen
Department of Resources Engineering,
National Cheng Kung University,
Tainan 71710,
Taiwan

Meng-Wei Wan (corresponding author)
Department of Environmental Resources Management,
Chia-Nan University of Pharmacy and Science,
Tainan 71710,
Taiwan
E-mail: *peterwan@mail.cnu.edu.tw*

INTRODUCTION

The contamination of arsenic in natural waters has been well documented in many countries including Argentina, Bangladesh, China, Chile, India, Philippines, Thailand and Taiwan (Mandal & Suzuki 2002; Sharma & Sohn 2009; Hosono *et al.* 2010). The primary source of arsenic in groundwater has been attributed to natural processes like geochemical reactions, volcanic emissions and weathering of arsenic rocks and minerals (Kanel *et al.* 2005). Another important source of arsenic is via anthropogenic activities such as ceramic and glassware production, herbicide and pesticide manufacturing, petroleum refineries, metallurgical industry and tannery operation (Altundogan *et al.* 2002).

Arsenic, which is a metalloid, is considered to be the 20th most abundant trace element (Mandal & Suzuki 2002; Nidheesh & Anantha Singh 2017). In general, arsenic exists in four oxidation states including +5 (arsenate), +3 (arsenite), 0 (metallic arsenic) and −3 (arsenide). Inorganic arsenic species such as arsenite [As(III)] and arsenate [As(V)] are commonly found in the aqueous environment, and are considered to be more toxic that the organic counterpart (Nidheesh & Anantha Singh 2017; Su *et al.* 2017). Detrimental health effects including disorder of the peripheral vascular system and central nervous system, peripheral neuropathy, conjunctivitis, gangrene, cardiovascular diseases and skin cancer have been related to long-term arsenic exposure (Bhattacharya *et al.* 2007). Moreover, the World Health Organization (WHO) categorized this element as a Class I human carcinogen (van Halem *et al.* 2009). Therefore, strict regulations have been implemented by WHO and the US Environmental Protection Agency where the current permissible limit of arsenic in drinking water is 10 μg/L (Smith *et al.* 2002). Meanwhile, Mexico

doi: 10.2166/wst.2018.339

and Taiwan have set the maximum contaminant level of arsenic for drinking water to be 25 and 10 μg/L, respectively (Chen & Chung 2006; Saldaña-Robles *et al.* 2017).

Adsorption is one of the most popular technologies utilized in the removal of heavy metals from waste effluents due to its simplicity in operation, low cost, safe handling, effectiveness even at a low concentration of contaminant, and applicability as a small-scale household module or in a community plant (Siddiqui & Chaudhry 2017). Adsorbents such as magnetite/non-oxidative graphene (Yoon *et al.* 2017), iron-coated seaweeds (Vieira *et al.* 2017), Fe_3O_4-GO-LDH (Wu *et al.* 2011), Fe_3O_4-GO (Sheng *et al.* 2012), chitosan-coated bentonite (CCB) (Arida *et al.* 2015) and perilla leaf biochar (Niazi *et al.* 2018) have been previously reported regarding the treatment of arsenic-contaminated waters.

The utilization of bentonite, chitosan, kaolinite and sand, which are natural and readily available materials, as inexpensive, eco-friendly adsorbents is considered to be a sustainable approach when utilized in environmental remediation technology. Chitosan is derived from the deacetylation of chitin, which is extracted from the shells of shrimps, krills, crayfish and crabs (Kumari *et al.* 2017). The shrimp and fish industry generate crustacean waste residue composed of heads, shells and tails, which is 40–50% by weight of the total solid waste (Ogawa *et al.* 2007). Clay materials are often produced by mining industries and major civil infrastructure construction projects as overburden or waste rock (Ocak 2009; Lu & Cai 2012). Bentonite is a smectite-type of clay characterized by its 2:1 layered aluminosilicate sheets (Zhang *et al.* 2016) while kaolinite, $Si_4Al_4O_{10}(OH)_8$, has a 1:1 layered structure (Bhattacharyya & Gupta 2008). On the other hand, silica sand is an abundant, cost-effective material with properties such as hardness and resistance to heat and chemicals (Ramakrishna *et al.* 2006; Sundararajan *et al.* 2009).

Several studies have examined the use of CCB, chitosan-coated sand (CCS) and chitosan-coated kaolinite (CCK) in the removal of various contaminants from wastewaters due to better chemical and mechanical stability, improved surface area and enhanced porosity of the adsorbent hybrid (Wan *et al.* 2004; Dalida *et al.* 2011; Futalan *et al.* 2011; Calagui *et al.* 2014; Arida *et al.* 2015; Chen *et al.* 2015; Ligaray *et al.* 2018). Moreover, coating chitosan onto a support material reduces the volume of chitosan required while retaining the overall adsorption efficiency (Wan *et al.* 2004). The work of Arida *et al.* (2015) determined that the uptake capacity at breakthrough of As(V) is 10.57 μg/g under fixed-bed conditions. However, a comparative study on adsorption efficiency using CCB, CCK and CCS in the removal of arsenic under static conditions has not yet been reported.

The present study aims at evaluating the capacity of CCB, CCK and CCS for adsorption of As(V) from aqueous solution. Adsorbents were characterized using scanning electron microscopy (SEM), thermogravimetric analysis (TGA), Fourier transform infrared spectroscopy (FT-IR) and the Brunauer–Emmett–Teller (BET) multipoint technique. Kinetic studies were performed to determine the rate-limiting step of the adsorption system using pseudo-first order, pseudo-second order and intraparticle diffusion equations. Thermodynamic and equilibrium studies were also carried out.

MATERIALS AND METHOD

Chemicals and materials

Low molecular weight chitosan (75–85% deacetylation), bentonite and kaolinite were purchased from Sigma-Aldrich (USA). Potassium iodide and hydrochloric acid (37% fuming) were acquired from Merck (Germany) while sand was obtained from Aquatek (Taiwan). Vitamin C and *di*-sodium hydrogen arsenate 7-hydrate ($Na_2HAsO_4{\cdot}7H_2O$) were purchased from Fisher Chemical (UK) and PanReac Applichem (Japan), respectively. All reagents obtained are of analytical grade and used without further purification.

Synthesis of CCB, CCK and CCS

The preparative method utilized was similar to that of Wan *et al.* (2004) with some modifications. Chitosan (5 g) was dissolved in 300 mL of 5% (v/v) HCl by stirring for 2 h. Then, 100 g support material was added into the mixture and was stirred for 3 h. Addition of 1 M NaOH into the mixture was performed in a drop-wise method until pH 7 was attained. Adsorbent beads were washed with deionized water, filtered and dried in an oven (Channel Oven, DV452) for 24 h at 65 °C. Adsorbents with a particle size range of 0.21 to 0.50 mm were utilized in the experiments.

Characterization

The morphology of the adsorbents was observed using SEM (S-3000N Hitachi, Japan) with a voltage of 20 kV under a

vacuum atmosphere of 1.33×10^{-6} mBar. The surface area and porosity of the adsorbents were determined using a BET surface analyzer (Micromeritics ASAP 2010, USA) at 77 K under N_2 gas. TGA was carried out using a thermo-mechanical analyzer (Perkin Elmer Pyris TGA-4000, USA) with a heating rate of 10 °C min^{-1} within the range of 30 to 800 °C. The spectra of chitosan, clay materials, sand, CCB, CCK and CCS were determined using FT-IR (Nicolet 6700) in the range of 400 to 4,000 cm^{-1}.

Batch adsorption study

Adsorption tests were carried out where 1 g adsorbent and 30 mL As(V) solution were agitated at 50 rpm using a reciprocal shaker bath (YIH-DER-BT 350, Taiwan) at 25 °C and pH 7.0 under varying initial concentration (50 to 1,000 μg/L) and contact time (0.5 to 24 h). Thereafter, the solution was filtered through a 0.45 μm cellulose filter and the filtrate was analyzed using an inductively coupled plasma optical spectroscopy (ICP-OES, Perkin Elmer Optima 2000 DV, USA).

Data analysis

The adsorption capacity at equilibrium, q_e (mg/g) was computed using Equation (1):

$$q_e = \frac{(C_0 - C_e) \times V}{M} \tag{1}$$

where V is the solution volume (mL), M is the adsorbent mass (g), C_0 and C_e refers to the initial and equilibrium concentration (mg/L), respectively.

To determine the rate-determining step of the adsorption system, kinetic equations are applied. The pseudo-first order (Lagergren 1898), pseudo-second order (Ho & McKay 1999) and intraparticle diffusion (Weber & Morris 1963) equations are expressed as the following:

$$\log (q_e - q_t) = \frac{k_1}{2.303} t + \log q_e \tag{2}$$

$$\frac{t}{q_t} = \frac{t}{q_e} + \frac{1}{k_2 q_e^2} \tag{3}$$

$$q_t = k_{id} t^{0.5} + C \tag{4}$$

where q_t (mg/g) denotes the adsorption capacity at time t (min), k_{id} (mg/g•$min^{0.5}$) denotes the rate constant of the intraparticle diffusion model, C refers to the thickness of the boundary layer (mg/g), and k_1 (1/min) and k_2 (g/mg•min) refer to the kinetic rate constants of the pseudo-first and pseudo-second order equation, respectively.

Equilibrium data are fitted using Langmuir, Freundlich and Dubinin-Radushkevich (D-R) isotherms, which are written as Equations (5) to (9):

$$\frac{1}{q_e} = \frac{1}{K_L q_m C_e} + \frac{1}{q_m} \tag{5}$$

$$\log q_e = \log K_F + \frac{1}{n} \log C_e \tag{6}$$

$$\ln q_e = \ln q_{DR} - \beta \varepsilon^2 \tag{7}$$

$$E = \frac{1}{\sqrt{2\beta}} \tag{8}$$

$$\varepsilon = RT \ln \left(1 + \frac{1}{C_e}\right) \tag{9}$$

where q_m refers to the maximum adsorption capacity at monolayer coverage (mg/g), K_L is the Langmuir constant that refers to the heat of adsorption (L/mg), $1/n$ refers to the linearity of adsorption (L/mg), K_F is the Freundlich adsorption capacity of the adsorbent (mg/g), q_{DR} is the D-R monolayer adsorption capacity (mg/g), β refers to the D-R constant regarding the mean free energy of the adsorbent (mol^2/kJ^2), E is the free energy of adsorption (kJ/mol), ε refers to the Polanyi potential (mol/kJ), R is the empirical gas constant (8.314 J/mol•K), and T is the operating temperature (K). The Langmuir isotherm assumes a monolayer adsorption occurring onto binding sites with homogenous energy levels where no further adsorption takes place at occupied sites (Langmuir 1918). The Freundlich isotherm, which is based on an empirical equation, refers to the adsorption of a solid adsorbent with energetically heterogeneous surfaces (Freundlich 1906; Wan Ngah & Fatinathan 2008). Meanwhile, the D-R isotherm is derived from the adsorption of sub-critical vapors on energetically irregular surfaces (Dubinin & Radushkevich 1947).

Linear and non-linear methods were used in evaluating the kinetic and equilibrium data. In Microsoft Excel, the *Solver add in* function was utilized in data analysis using non-linear equations. The linear form of the models was assessed using the linear regression method.

Error analysis

Error functions are used in order to evaluate the fit of the kinetic and isotherm equations with the experimental data.

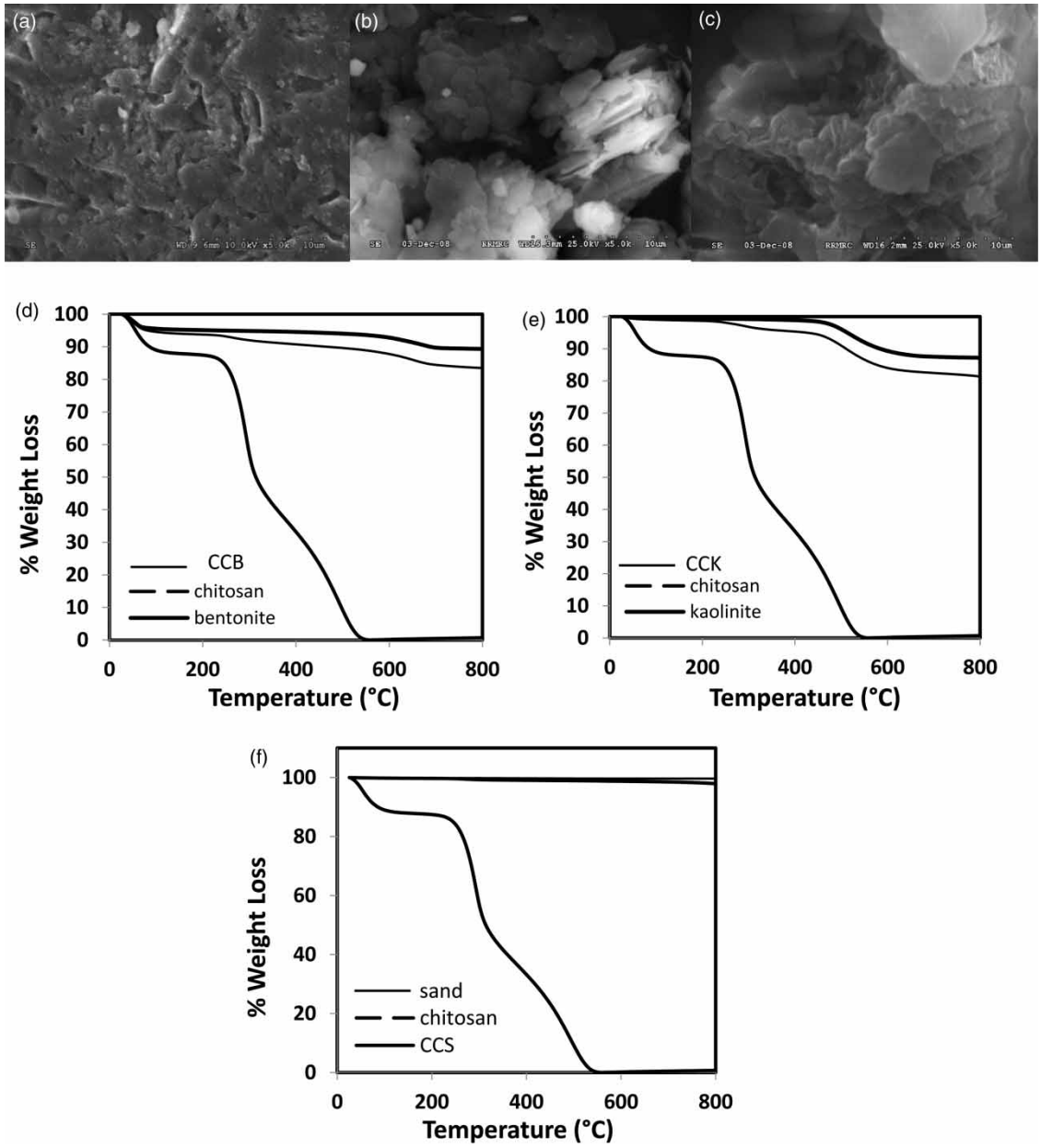

Figure 1 | Characterization analysis illustrating the SEM images of (a) CCS, (b) CCK and (c) CCB and TGA of (d) CCB, chitosan and bentonite, (e) CCK, chitosan and kaolinite, and (f) CCS, chitosan and sand.

The sum of squares error (*SSE*) and root means square error (*RMSE*) were computed using Equations (10) and (11) (Karri *et al.* 2017):

$$SSE = \sum_{i=1}^{n} |q^i_{e,\exp l} - q^i_{e,theor}| \quad (10)$$

$$RMSE = \sqrt{\frac{1}{n-1}\sum_{i=1}^{n} (q^i_{e,theor} - q^i_{e,\exp l})^2} \quad (11)$$

where n is the number of observations, $q^i_{e,expl}$ refers to the measured concentration (μg/L) and $q^i_{e,theor}$ stands for the predicted value of the model (μg/L).

RESULTS AND DISCUSSION

Characterization

Figure 1(a) to 1(c) illustrate the surface morphology of CCS, CCK and CCB. The surface irregularity and roughness of the

adsorbents can be arranged in the following order: CCB > CCK > CCS. Moreover, CCS has a smoother exterior morphology with few ridges and wrinkles covering its surface, while CCB and CCK displayed aggregation with a coarse surface.

Based on BET analysis, both chitosan and CCK were determined to be mesoporous materials while CCB and CCS exhibited macroporosity. Pure chitosan displayed a low surface area (2.12 m^2/g), pore volume (0.032 cm^3/g) and diameter (11.61 nm) while coating chitosan onto a support material resulted in a higher BET surface area, pore volume and average pore diameter for CCB (9.22 m^2/g, 0.048 cm^3/g, 80.54 nm) and CCK (5.52 m^2/g, 0.035 cm^3/g, 29.98 nm). Among the adsorbents, CCS showed the least surface area (0.47 m^2/g) and pore volume (0.004 cm^3/g) but has the largest average pore diameter (683.80 nm).

Figure 1(d) to 1(f) illustrate the TGA curves of CCB, CCK and CCS. In general, chitosan displayed a weight loss of 12% that occurred between 70 °C to 97 °C, which is attributed to loss of physically adsorbed water. The second and third decomposition stages occurred between 232 °C to 550 °C and were due to decomposition of the chitosan backbone such as D-glucosamine and *N*-acetylglucosamine (Soon *et al.* 2018). Then, chitosan was burnt out completely at 550 °C.

For bentonite, 5% weight loss at <100 °C was due to loss of physically adsorbed water molecules in the interlayer (Figure 1(d)). A second weight loss of 4% at 400 °C to 700 °C was attributed to the evaporation of water molecules contained within the crystal lattice (Belbachir & Makhoukhi 2017). Figure 1(e) illustrates two decomposition stages of kaolinite: 2% loss at 200 °C to 470 °C and 6% loss at

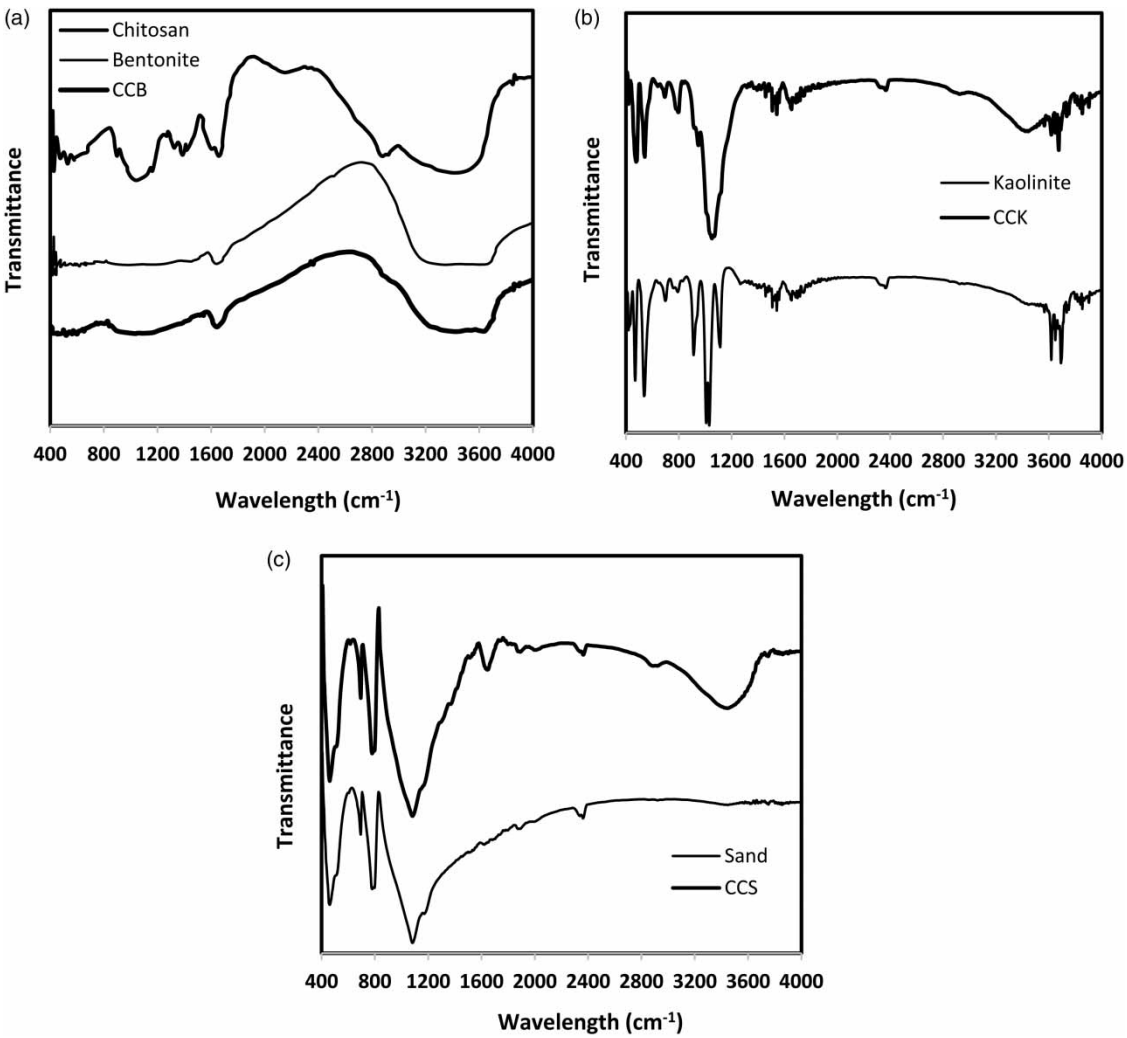

Figure 2 | FT-IR spectra of (a) bentonite, chitosan, and CCB; (b) CCK and kaolinite; and (c) CCS and sand.

470 °C to 620 °C due to physically adsorbed water and dihydroxylation of kaolinite samples, respectively (Drweesh *et al.* 2016). Meanwhile, sand displayed only 2% weight loss starting at 80 °C due to loss of physically adsorbed water (Figure 1(f)). The curves of CCB, CCK and CCS are a combination of degradation profiles of chitosan and the support materials. When compared with the support materials' profile, the weight loss observed were higher such as 10%, 15% and 2.5% for CCB, CCK and CCS, respectively. Based on the TGA curves, 4.7%, 4.8% and 2.1% of chitosan were coated onto bentonite, kaolinite and sand, respectively.

Figure 2 illustrates several peaks that are attributed to chitosan: 3,411 cm^{-1} refers to the primary amine and hydroxyl groups stretching vibration, 2,808 cm^{-1} refers to the stretching of C-H in CH_2 groups, 1,414 cm^{-1} refers to

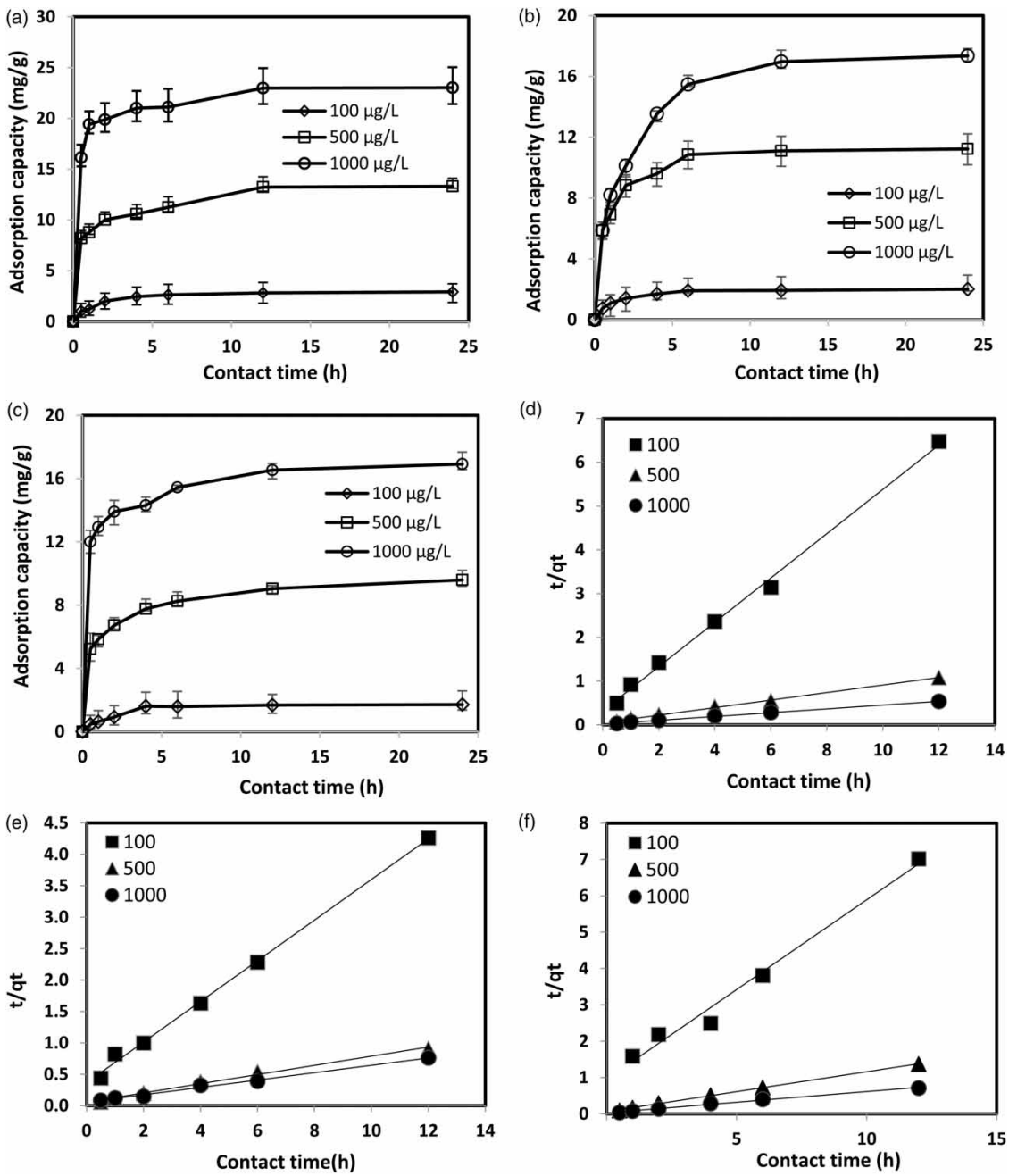

Figure 3 | Effect of contact time on As(V) adsorption capacity of (a) CCB, (b) CCK and (c) CCS and the pseudo-second order kinetic plots of (d) CCB, (e) CCK and (f) CCS.

the –N-H amide stretching and 1,077 cm^{-1} is due to stretching vibration of C-OH (Zhang *et al.* 2012; Cao *et al.* 2014; Igberase *et al.* 2014). The spectrum of bentonite shows bands at 3,411 and 828 cm^{-1} that refer to the stretching vibration of –OH and Al-O groups, respectively (Huang *et al.* 2017). From the kaolinite spectrum, peaks at 541 and 468 cm^{-1} refer to bending vibrations of Al-O-Si and Si-O-Si, 914 cm^{-1} refers to the inner surface –OH bending, 1,039 cm^{-1} is due to the apical Si-O stretching, and 3,618 cm^{-1} refers to the stretching vibration of the inner Al-OH group (Fatimah 2018). In sand, the peak at 1,086 cm^{-1} refers to the Si-O-Si bridge asymmetric stretching, and peaks at 795 and 690 cm^{-1} are due to symmetric stretching of Si-O bridging oxygen atoms (Chaudhry *et al.* 2017). The spectra of the composite materials demonstrate the presence of several peaks that are mainly attributed to the support material (bentonite, kaolinite and sand) with a few bands contributed by chitosan including 3,441 to 3,660 cm^{-1} (N-H and O-H stretching), 2,912 to 2,936 cm^{-1} (C-H stretching) and 1,649 cm^{-1} (amine stretching) (Huang *et al.* 2016).

Kinetic study

As shown in Figure 3(a) to 3(c), results displayed a rapid initial uptake of As(V) within 2 h that could be attributed to the availability of numerous adsorption sites. At an initial As(V) concentration of 1,000 μg/L, adsorption capacity of 23.02, 17.35 and 16.92 mg/g was attained for CCB, CCK

Table 1 | Kinetic parameters derived using linear regression method for the adsorption of As(V) by CCB, CCK and CCS

			Adsorbent		
Model	**Initial concentration**	**Parameters**	**CCB**	**CCK**	**CCS**
Pseudo-first order	100	k_1	0.1785	0.2546	0.5122
		q_1	1.24	1.69	1.83
		R^2	0.6618	0.9514	0.8532
		RMSE	8.2471	14.0599	12.6801
	500	k_1	0.3183	0.2612	0.1707
		q_1	4.72	8.51	5.13
		R^2	0.9617	0.9215	0.9799
		RMSE	6.2270	15.6020	16.9264
	1000	k_1	0.2079	0.3551	0.1451
		q_1	7.26	8.26	4.32
		R^2	0.9623	0.9562	0.7763
		RMSE	18.8478	9.1224	12.9304
Pseudo-second order	100	k_2	0.7771	0.3237	0.2603
		q_2	3.15	2.75	1.05
		R^2	0.9970	0.9974	0.9847
		RMSE	5.0440	6.0775	3.1382
	500	k_2	0.5622	0.1690	0.1527
		q_2	20.45	18.68	15.80
		R^2	0.9983	0.9927	0.9993
		RMSE	4.0903	7.2969	7.2902
	1000	k_2	0.1038	0.0899	0.0211
		q_2	54.35	18.02	35.59
		R^2	0.9991	0.9934	0.9952
		RMSE	8.2272	6.0555	9.1833
Intraparticle diffusion	100	k_{id}	0.3462	0.8147	0.3097
		R^2	0.8264	0.9484	0.7927
		RMSE	16.8871	21.7228	18.7336
	500	k_{id}	0.6258	0.7522	0.5853
		R^2	0.8801	0.9606	0.9204
		RMSE	22.2578	24.9178	13.8562
	1000	k_{id}	0.4987	0.413	0.846
		R^2	0.8564	0.7522	0.9127
		RMSE	15.6356	11.0741	21.9178

and CCS, respectively. After which, adsorption capacity was observed to increase slowly until equilibrium was attained in 4 h at 100 μg/L and 12 h at 500 and 1,000 μg/L. A low concentration would indicate that there is less amount of As(V) present in the solution, hence there is less competition and ions bind easily onto the adsorbent. At higher concentration, the effect of steric crowding becomes more significant since there would be shorter distances between As(V) ions present in the solution, where repulsive forces would be exerted between ions, which would contribute to the delay in the attainment of equilibrium.

Based on Table 1 and 2, the high values of the coefficient of determination (R^2) for CCB ($R^2 \geq 0.9970$), CCK ($R^2 \geq 0.9923$) and CCS ($R^2 \geq 0.9847$) derived from linear and non-linear equation indicate a good correlation between the experimental and predicted data generated by the pseudo-second order equation. Figure 3(d) to 3(f) display the goodness of fit of the experimental data with the linear plots generated by the pseudo-second order model. Moreover, the low error values of *RMSE* for CCB, CCK and CCS further validate that the pseudo-second order equation best describes the adsorption system. This implies that the rate-determining step is chemisorption, wherein a covalent bond is formed through sharing a pair of electrons between As(V) and the active sites of the adsorbents. It is observed that the non-linear equations provided lower *RMSE* error values and higher R^2 values in comparison to the linear equation.

Under all concentration ranges studied, the highest k_2 constant occurred with CCB followed by CCK and CCS.

Table 2 | Kinetic parameters derived using non-linear method for the adsorption of As(V) by CCB, CCK and CCS

			Adsorbent		
Model	**Initial concentration**	**Parameters**	**CCB**	**CCK**	**CCS**
Pseudo-first order	100	k_1	0.1293	0.2498	0.5021
		q_1	2.68	1.73	1.08
		R^2	0.6975	0.9320	0.8861
		RMSE	8.8183	9.1224	11.3299
	500	k_1	0.3692	0.2164	0.2150
		q_1	6.80	5.38	4.85
		R^2	0.9026	0.8252	0.9275
		RMSE	12.6801	9.9294	10.0586
	1000	k_1	0.2131	0.3298	0.1237
		q_1	9.44	7.45	5.57
		R^2	0.9224	0.9614	0.9036
		RMSE	8.0555	12.2584	9.1157
Pseudo-second order	100	k_2	0.7511	0.3222	0.2751
		q_2	3.99	3.17	1.91
		R^2	0.9994	0.9923	0.9987
		RMSE	5.7640	7.0576	5.0435
	500	k_2	0.5063	0.1726	0.1382
		q_2	22.84	16.87	14.77
		R^2	0.9998	0.9936	0.9987
		RMSE	8.3245	7.8318	6.6386
	1000	k_2	0.1097	0.0775	0.0138
		q_2	52.83	19.02	33.91
		R^2	0.9991	0.9952	0.9947
		RMSE	5.6386	2.2458	7.1247
Intraparticle diffusion	100	k_{id}	0.3462	0.8147	0.3097
		R^2	0.8264	0.9484	0.7927
		RMSE	25.4516	19.2272	16.4939
	500	k_{id}	0.6258	0.7522	0.5853
		R^2	0.8258	0.9365	0.9072
		RMSE	16.8760	24.9178	14.2158
	1000	k_{id}	0.4987	0.413	0.846
		R^2	0.8635	0.7822	0.8910
		RMSE	20.8179	15.0710	18.2584

The high rate constant of CCB would imply rapid adsorption rates and high adsorption capacity. For all adsorbents, the kinetic rate constant, k_2, was observed to decrease as the initial concentration was increased from 100 to 1,000 μg/L. This denotes that there is tighter competition between ions at high concentration that leads to a lower rate constant and decreased adsorption capacity.

Isotherm study

Based on Table 3, the high R^2 values ($R^2 \geq 0.9753$) and low error values of *SSE* and *RMSE* imply that the Langmuir isotherm best describes the adsorption system. This denotes that uptake of As(V) by CCB, CCK and CCS occurs as a monolayer coverage onto binding sites with homogenous sorption energies. Results show that the parameters derived from linear and non-linear equations do not have the same values. The discrepancy in the values is attributed to the use of linear equations (Narayanan *et al.* 2017). However, the parameters displayed a similar trend whether linear or non-linear equations were utilized. The values of the Langmuir constant q_m can be arranged in the order: CCB > CCK > CCS, where the high adsorption capacity of CCB can be attributed to its high surface area and large pore diameter. Hence, the preferential adsorption of As(V) is due to the higher number of binding sites available for CCB. Moreover, a larger pore diameter would mean accessibility of As(V) with a thermochemical radius of 0.248 nm into the pore network, which results in better adsorption rates (Chen *et al.* 2004).

The Freundlich constant n would indicate whether the adsorption process is chemical ($n < 1$) or physical ($n > 1$) in nature (Veli & Alyuz 2007). For CCB, CCK and CCS, the n values were determined to be within the range of 1.225 to 2.303, which implies that the adsorption system is physical in nature. Figure 4(a) to 4(c) illustrate the Freundluch, Langmuir and D-R models plotted against the experimental data. A good correlation is observed between experimental and predicted data generated by the Langmuir model, which further validates that Langmuir is the most appropriate isotherm to describe the adsorption process in the present work.

Among the isotherm models applied, D-R provided the lowest R^2 values ($R^2 \leq 0.9658$) and high error values ($RMSE \geq 8.5436$; $SSE \geq 12.8545$) that signifies unsatisfactory correlation between predicted and experimental data. The D-R constant E describes the change in free energy when a mole of adsorbate from solution diffuses onto the adsorbent surface (Chen *et al.* 2008). Its value provides information on whether the adsorption behavior is related to physical adsorption ($E < 8$ kJ/mol), ion-exchange mechanism (8 kJ/mol $< E <$ 16 kJ/mol) or chemisorption ($E > 16$ kJ/mol). The values obtained for CCB, CCK and CCS lie within the range of 0.017 to 0.143 kJ/mol, which indicates that physical adsorption predominates in the uptake of As(V).

Table 3 | Parameters derived from isotherm models for adsorption of As(V) by CCB, CCK and CCS using linear and non-linear methods

		Adsorbent					
		CCB		CCK		CCS	
Isotherm	Parameters	Linear	Non-linear	Linear	Non-linear	Linear	Non-linear
Langmuir	q_m (mg/g)	67.11	62.64	64.85	58.01	16.78	21.73
	K_L (L/mg)	0.008	0.001	0.002	0.003	0.001	0.010
	R^2	0.9832	0.9921	0.9753	0.9985	0.9986	0.9897
	SSE	16.2651	12.2111	5.4763	1.5194	1.1979	0.3262
	RMSE	3.0122	5.5081	3.0385	6.6053	8.5123	3.0651
Freundlich	K_F (mg/g)	3.11	3.36	2.54	3.02	1.39	0.94
	n (mg/L)	1.225	1.628	1.473	1.517	1.713	2.030
	R^2	0.9120	0.9312	0.9597	0.9686	0.9823	0.9483
	SSE	28.8450	13.9930	9.5904	3.9287	12.2457	8.5011
	RMSE	11.6788	9.3818	6.5176	12.7548	9.8239	12.3490
D-R	q_{DR} (mg/g)	12.79	13.05	11.87	14.16	10.58	11.88
	E (kJ/mol)	0.017	0.035	0.081	0.143	0.082	0.079
	R^2	0.9658	0.9632	0.8611	0.8978	0.7974	0.8292
	SSE	24.1716	12.8545	35.2093	30.9167	18.4171	15.3262
	RMSE	8.9632	15.8653	10.1767	21.7141	8.5436	11.5561

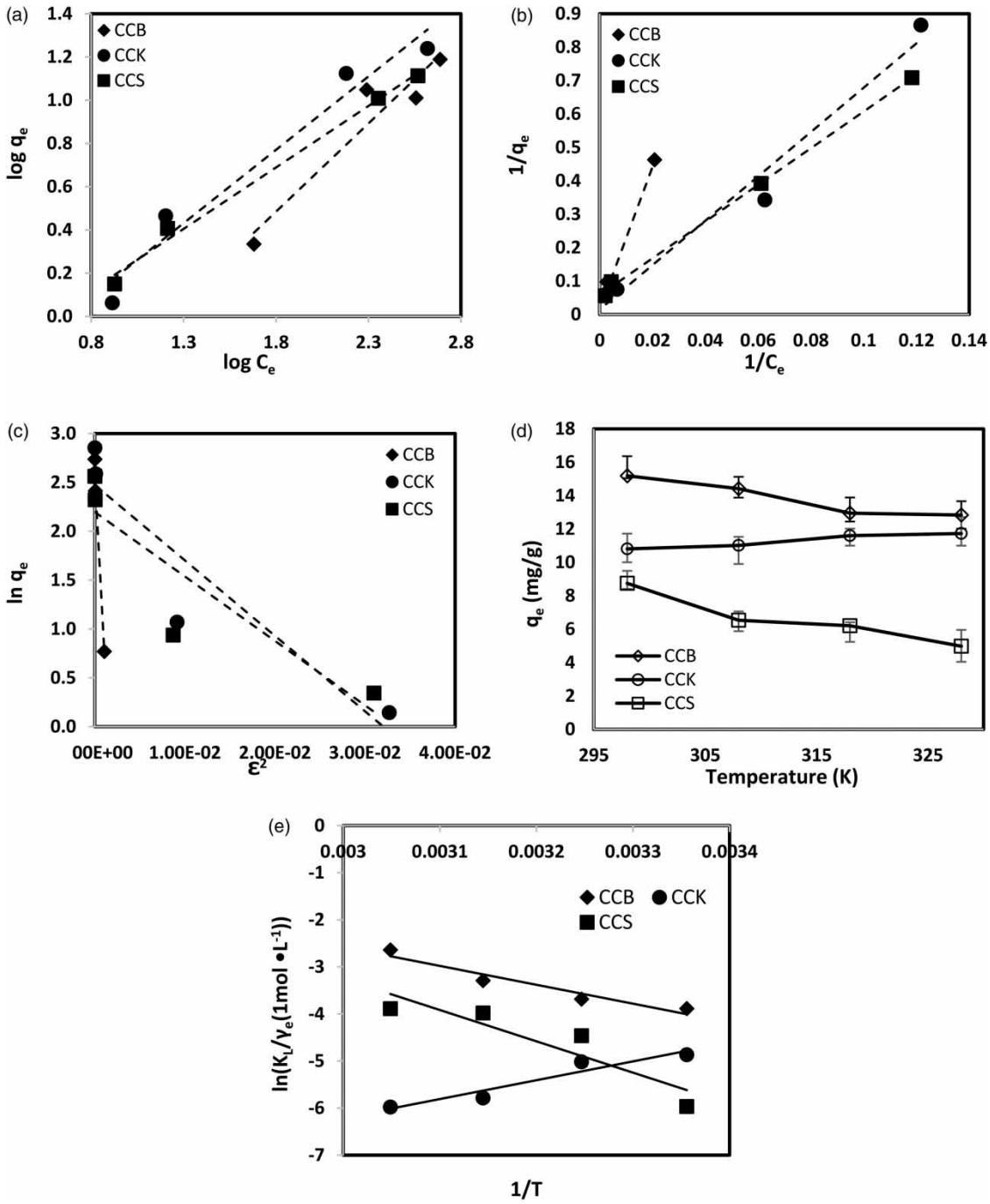

Figure 4 | Adsorption isotherms using (a) Freundlich, (b) Langmuir and (c) D-R equation and the plots of (d) effect of temperature and (e) van 't Hoff equation on As(V) adsorption using CCB, CCK and CCS.

In Table 4, the As(V) adsorption capacity of CCB, CCK and CCS was compared with various other adsorbents reported in the literature. Among the adsorbents, Fe_3O_4-GO-LDH provided the highest adsorption capacity followed by CCB and CCK. It is essential to emphasize that CCB and CCK are derived from low cost and readily available materials when compared to Fe_3O_4-GO-LDH, where the latter would require a more complicated fabrication procedure. Results indicate that CCB and CCK can be applied as low-cost adsorbents in removing As(V) from waste effluents under neutral conditions.

Table 4 | Comparison of As(V) adsorption capacity of different adsorbents

Adsorbent	Surface area (m^2/g)	Adsorption capacity (mg/g)	Reference
Iron-coated seaweeds	———	7.30	Vieira *et al.* (2017)
Perilla leaf derived biochar	473.40	7.21	Niazi *et al.* (2018)
Fe_3O_4-GO	165.00	59.60	Sheng *et al.* (2012)
Fe_3O_4-GO-LDH	123.30	73.14	Wu *et al.* (2011)
Magnetite	189.94	9.44	Yoon *et al.* (2017)
CCS	0.47	16.78	This study
CCK	5.52	64.85	This study
CCB	9.22	67.11	This study

Thermodynamic study

The effect of temperature on the As(V) adsorption by CCB, CCK and CCS under varying temperature is shown in Figure 4(d). Results show that As(V) uptake increased from 10.81 to 11.72 mg/g as temperature was increased from 298 to 328 K for CCK while adsorption of As(V) decreased from 15.18 to 12.83 mg/g for CCB and from 8.75 to 4.98 mg/g for CCS with higher temperature.

Thermodynamic parameters such as standard Gibbs free energy (ΔG°, kJ/mol), enthalpy (ΔH°, kJ/mol) and entropy (ΔS°, kJ/mol•K) were calculated using Equations (12) to (14) (Liu 2009):

$$\Delta G^0 = -RT \ln\left[\frac{K_L}{\gamma_e}(1mol \bullet L^{-1})\right] \quad (12)$$

$$\log \gamma_e = -z^2 I_e^{1/2} \quad (13)$$

$$\ln\left[\frac{K_L}{\gamma_e}(1mol \bullet L^{-1})\right] = \frac{\Delta S^0}{R} - \frac{\Delta H^0}{RT} \quad (14)$$

where γ_e is the activity coefficient at equilibrium, z is the charge of As(V) and I_e is the ionic strength of As(V) at equilibrium. Equation (12) was utilized based on As(V) being a charged species under high concentration, where γ_e has been taken into account.

Based on Table 5, the negative values of ΔG^0 of CCB and CCS from 298 to 328 K indicate that the adsorption of As(V) proceeds spontaneously. Meanwhile, non-spontaneous adsorption occurs at 298 to 328 K for CCK. A more negative value of ΔG° would favor adsorption. Since

Table 5 | Thermodynamic parameters of As(V) adsorption by CCB, CCK and CCS

Adsorbent	Temperature (K)	ΔG^0 (kJ/mol)	ΔH^0 (kJ/mol)	ΔS^0 (J/mol•K)
CCB	298	−7.21	33.30	0.0785
	308	−8.71		
	318	−9.43		
	328	−9.63		
CCK	298	12.06	− 33.28	0.1514
	308	12.85		
	318	15.30		
	328	16.31		
CCS	298	−1.06	55.28	0.1388
	308	−1.43		
	318	−4.78		
	328	−6.21		

the value of ΔG° for CCB yields to be the most negative, adsorption using CCB was favored over CCK and CCS. For CCB and CCS, the values of ΔG^0 become more negative with increase in temperature, implying that adsorption is more feasible at higher temperatures. This implies that adsorption was more feasible at 328 K due increase in the diffusion rates of the As(V). On the other hand, ΔG^0 values of CCK were observed to become more positive at higher temperature. An increase in temperature could indicate less stable bonds between the binding sites and As(V), which led to decreased adsorption capacity (Yoon *et al.* 2017). In all adsorbents, the positive ΔS^0 values imply that there is an increase in randomness after adsorption of As(V) onto the adsorbent surface. Meanwhile, the negative value of ΔH^0 indicates that As(V) uptake onto CCK is exothermic in nature while As(V) uptake using CCB and CCS is an endothermic process.

CONCLUSIONS

In the present study, the viability of utilizing CCB, CCK and CCS in the uptake of As(V) from aqueous solution was evaluated. Equilibrium data of the three adsorbents were fitted using the linear and non-linear isotherm models. Results show that the data correlated well with the Langmuir isotherm, which indicates that As(V) adsorption occurs at a monolayer coverage onto binding sites with homogenous energy levels. Based on both linear and non-linear methods, low values of error functions ($RMSE \leq 8.5123$; $SSE \leq 16.2651$) with high R^2 values (≥ 0.9753) were attained for the Langmuir isotherm. At pH 7.0 and 298 K, the maximum adsorption capacity derived from the Langmuir model was determined to be 67.11, 64.85, and 16.78 mg/g for CCB,

CCK and CCS, respectively. In addition, the obtained values are comparable or higher than the values of various adsorbents reported in the literature. CCB was shown to have the highest adsorption capacity for As(V) over CCK and CCS, which suggests easily accessible and higher number of available binding sites due to its high surface area and large pore diameter. The E values (0.017 to 0.143 kJ/mol) derived from the D-R isotherm imply that the adsorption process is governed by physical adsorption. High R^2 values ($\geq$0.9847) and low error function values ($RMSE \leq 9.1833$) indicate that the pseudo-second order equation best describes the kinetic data of As(V) adsorption. This denotes that chemisorption is the rate-limiting step of the adsorption system. Adsorption of As(V) results in an increase in the randomness at the solution-solid interface. Moreover, adsorption of As(V) by CCK is exothermic in nature and endothermic for CCB and CCS. This study demonstrated the feasibility of using CCB and CCK for the removal of As(V) from water.

ACKNOWLEDGEMENTS

The authors thank the Ministry of Science and Technology, Taiwan (MOST 105-2221-E-041-002-MY3) and the National Research Foundation (NRF) of Korea through the Ministry of Education (No. 2016R1A6A1A03012812) for providing financial support for this research undertaking.

REFERENCES

Altundogan, H. S., Altundogan, S., Tumen, F. & Bildik, M. 2002 Arsenic adsorption from aqueous solutions by activated red mud. *Waste Management* **22** (3), 357–363.

Arida, C. V. J., de Luna, M. D. G., Futalan, C. M. & Wan, M. W. 2015 Optimization of As(V) removal using chitosan-coated bentonite from groundwater using Box-Behnken design: effects of adsorbent mass, flow rate, and initial concentration. *Desalination and Water Treatment* **57** (40), 18739–18747.

Belbachir, I. & Makhoukhi, B. 2017 Adsorption of Bezathren dyes onto sodic bentonite from aqueous solutions. *Journal of the Taiwan Institute of Chemical Engineers* **75**, 105–111.

Bhattacharyya, K. G. & Gupta, S. S. 2008 Adsorption of a few heavy metals on natural and modified kaolinite and montmorillonite: a review. *Advances in Colloid and Interface Science* **140**, 114–131.

Bhattacharya, P., Welch, A. H., Stollenwerk, K. G., McLaughlin, M. J., Bundschuh, J. & Panaullah, G. 2007 Arsenic in the environment: biology and chemistry. *Science of the Total Environment* **379** (2–3), 109–120.

Calagui, M. J. C., Senoro, D. B., Kan, C. C., Salvacion, J. W. L., Futalan, C. M. & Wan, M. W. 2014 Adsorption of indium(III) ions from aqueous solution using chitosan-coated beads. *Journal of Hazardous Materials* **277**, 120–126.

Cao, C., Xiao, L., Chen, C., Shi, X., Cao, Q. & Cao, L. 2014 In situ preparation of magnetic Fe_3O_4/chitosan nanoparticles via a novel reduction-precipitation method and their application in adsorption of reactive azo dye. *Powder Technology* **260**, 90–97.

Chaudhry, S. A., Zaidi, Z. & Siddiqui, S. I. 2017 Isotherm, kinetic and thermodynamics of arsenic adsorption onto Iron-Zirconium Binary Oxide-Coated Sand (IZBOCS): modelling and process optimization. *Journal of Molecular Liquids* **229**, 230–240.

Chen, C. C. & Chung, Y. C. 2006 Arsenic removal using a biopolymer chitosan sorbent. *Journal of Environmental Science and Health, Part A* **41** (4), 645–658.

Chen, N., Lu, W., Yang, J. & Li, G. 2004 *Support Vector Machine in Chemistry*. World Scientific Publishing Co. Pte. Ltd, Singapore.

Chen, A. W., Liu, S. C., Chen, C. Y. & Chen, C. Y. 2008 Comparative adsorption of Cu(II), Zn(II) and Pb(II) ions in aqueous solution on the crosslinked chitosan with epichlorohydrin. *Journal of Hazardous Materials* **154** (1–3), 184–191.

Chen, I. P., Kan, C. C., Futalan, C. M., Calagui, M. J. C., Lin, S. S., Tsai, W. C. & Wan, M. W. 2015 Batch and fixed bed studies: removal of copper(II) using chitosan-coated kaolinite beads from aqueous solution. *Sustainable Environment Research* **25** (2), 73–81.

Dalida, M. L. P., Mariano, A. F. V., Futalan, C. M., Kan, C. C., Tsai, W. C. & Wan, M. W. 2011 Adsorptive removal of Cu(II) from aqueous solution using non-crosslinked and crosslinked chitosan-coated bentonite beads. *Desalination* **275**, 154–159.

Drweesh, S. A., Fathy, N. A., Wahba, M. A., Hanna, A. A., Akarish, A. I. M., Elzahany, E. A. M., El-Sherif, I. Y. & Abou-El-Sherbini, K. S. 2016 Equilibrium, kinetic and thermodynamic studies of Pb(II) adsorption from aqueous solutions on HCl-treated Egyptian kaolin. *Journal of Environmental Chemical Engineering* **4** (2), 1674–1684.

Dubinin, M. M. & Radushkevich, L. V. 1947 The equation of the characteristic curve of the activated charcoal. *Proceedings of the USSR Academy of Sciences Physical Chemistry* **55**, 331–337.

Fatimah, I. 2018 Preparation, characterization and physicochemical study of 3-amino propyl trimethoxy silane-modified kaolinite for Pb(II) adsorption. *Journal of King Saud University – Science* **30**, 250–257.

Freundlich, H. M. 1906 Over the adsorption in solution. *Journal of Physical Chemistry A* **57**, 385–470.

Futalan, C. M., Kan, C. C., Dalida, M. L., Hsien, K. J., Pascua, C. & Wan, M. W. 2011 Comparative and competitive adsorption of copper, lead and nickel using chitosan immobilized on bentonite. *Carbohydrate Polymers* **83**, 528–536.

Ho, Y. S. & McKay, G. 1999 Pseudo-second order model for sorption processes. *Process Biochemistry* **34**, 451–465.

Hosono, T., Siringan, F., Yamanaka, T., Umezawa, Y., Onodera, S., Nakano, T. & Taniguchi, M. 2010 Application of multi-isotope ratios to study the source and quality of urban groundwater in Metro Manila, Philippines. *Applied Geochemistry* **25** (6), 900–909.

Huang, R., Zhang, L., Hu, P. & Wang, J. 2016 Adsorptive removal of Congo red from aqueous solutions using crosslinked chitosan and crosslinked chitosan immobilized bentonite. *International Journal of Biological Macromolecules* **86**, 496–504.

Huang, Z., Li, Y., Chen, W., Shi, J., Zhang, N., Wang, X., Li, Z., Gao, L. & Zhang, Y. 2017 Modified bentonite adsorption of organic pollutants of dye wastewater. *Materials Chemistry and Physics* **202**, 266–276.

Igberase, E., Osifo, P. & Ofomaja, A. 2014 The adsorption of copper(II) ions by polyaniline graft chitosan beads from aqueous solution: equilibrium, kinetic and desorption studies. *Journal of Environmental Chemical Engineering* **2**, 362–369.

Kanel, S. R., Manning, B., Charlet, L. & Choi, H. 2005 Removal of arsenic (III) from groundwater by nanoscale zero-valent iron. *Environmental Science and Technology* **39** (5), 1291–1298.

Karri, R. R., Sahu, J. N. & Jayakumar, N. S. 2017 Optimal isotherm parameters for phenol adsorption from aqueous solutions onto coconut shell based activated carbon: error analysis of linear and non-linear methods. *Journal of the Taiwan Institute of Chemical Engineers* **80**, 472–487.

Kumari, S., Annamareddy, S. H. K., Abanti, S. & Rath, P. K. 2017 Physicochemical properties and characterization of chitosan synthesized from fish scales, crab and shrimp shells. *International Journal of Biological Molecules* **104**, 1697–1705.

Lagergren, S. Y. 1898 About the theory of so-called adsorption of soluble substances. *Kungliga Svenska Vetenskapsakademiens Handlingar* **24** (4), 1–39.

Langmuir, I. 1918 The adsorption of gases on plane surfaces of glass, mica and platinum. *Journal of the American Chemical Society* **40** (9), 1361–1403.

Ligaray, M., Futalan, C. M., de Luna, M. D. & Wan, M. W. 2018 Removal of chemical oxygen demand from thin-film transistor liquid-crystal display wastewater using chitosan-coated bentonite: isotherm, kinetics and optimization studies. *Journal of Cleaner Production* **175**, 145–154.

Liu, Y. 2009 Is the free energy change of adsorption correctly calculated? *Journal of Chemical & Engineering Data* **54**, 1981–1985.

Lu, Z. & Cai, M. 2012 Disposal methods on solid wastes from mines in transition from open-pit to underground mining. *Procedia Environmental Sciences* **16**, 715–721.

Mandal, B. K. & Suzuki, K. T. 2002 Arsenic round the world: a review. *Talanta* **58** (1), 201–235.

Narayanan, N., Gupta, S., Gajbhiye, V. T. & Manjaiah, K. M. 2017 Optimization of isotherm models for pesticide sorption on biopolymer-nanoclay composite by error analysis. *Chemosphere* **173**, 502–511.

Niazi, N. K., Bibi, I., Shahid, M., Ok, Y. S., Burton, E. D., Wang, H., Shaheen, S. M., Rinklebe, J. & Lüttge, A. 2018 Arsenic removal by perilla leaf biochar in aqueous solutions and groundwater: an integrated spectroscopic and microscopic examination. *Environmental Pollution* **232**, 31–41.

Nidheesh, P. V. & Anantha Singh, T. S. 2017 Arsenic removal by electrocoagulation process: recent trends and removal mechanism. *Chemosphere* **181**, 418–432.

Ocak, I. 2009 Environmental problems caused by Istanbul subway excavation and suggestions for remediation. *Environmental Geology* **58** (7), 15–57.

Ogawa, M., Maia, E. L., Fernandes, A. C., Nunes, M. L., Oliveira, M. I. & Freitas, S. T. 2007 Waste from processing of farmed shrimp: a source of carotenoid pigments. *Ciência E Tecnologia de Alimentos* **27** (2), 333–337.

Ramakrishna, D. M., Viraraghavan, T. & Jin, Y. 2006 Iron oxide coated sand for arsenic removal: investigation of coating parameters using a factorial design approach. *Practice Periodical of Hazardous, Toxic, and Radioactive Waste Management* **10** (4), 198–206.

Saldaña-Robles, A., Saldaña-Robles, N., Saldaña-Robles, A. L., Damian-Ascencio, C., Rangel-Hernandez, V. H. & Guerra-Sanchez, R. 2017 Arsenic removal from aqueous solutions and the impact of humic and fulvic acids. *Journal of Cleaner Production* **159**, 425–431.

Sharma, V. K. & Sohn, M. 2009 Aquatic arsenic: toxicity, speciation, transformations, and remediation. *Environment International* **35** (4), 743–759.

Sheng, G., Li, Y., Yang, X., Ren, X., Yang, S., Hu, J. & Wang, X. 2012 Efficient removal of arsenate by versatile magnetic graphene oxide composites. *RSC Advances* **2**, 12400–12407.

Siddiqui, S. I. & Chaudhry, S. A. 2017 Iron oxide and its modified forms as an adsorbent for arsenic removal: a comprehensive recent advancement. *Process Safety and Environmental Protection* **111**, 592–626.

Smith, A. H., Lopipero, P. A., Bates, M. N. & Steinmaus, C. M. 2002 Arsenic epidemiology and drinking water standards. *Science* **296** (5576), 2145–2146.

Soon, C. Y., Tee, Y. B., Tan, C. H., Rosnita, A. T. & Khalina, A. 2018 Extraction and physicochemical characterization of chitin and chitosan from *Zophobas morio* larvae in varying sodium hydroxide concentration. *International Journal of Biological Macromolecules* **108**, 135–142.

Su, H., Ye, Z. & Hmidi, N. 2017 High-performance iron oxide-graphene oxide nanocomposite adsorbents for arsenic removal. *Colloids and Surfaces A: Physicochemical and Engineering Aspects* **522**, 161–172.

Sundararajan, M., Ramaswamy, S. & Raghavan, P. 2009 Evaluation for the beneficiability of white silica sands from the overburden of lignite mine situated in Rajpardi district of Gujarat, India. *Journals of Minerals & Materials Characterization & Engineering* **8** (9), 701–714.

van Halem, D., Bakker, S. A., Amy, G. L. & van Dijk, J. C. 2009 Arsenic in drinking water: a worldwide water quality concern for water supply companies. *Drinking Water Engineering and Science* **2** (1), 29–34.

Veli, S. & Alyuz, B. 2007 Adsorption of copper and zinc from aqueous solutions by using natural clay. *Journal of Hazardous Materials* **149** (1), 226–233.

Vieira, B. R. C., Pintor, A. M. A., Boaventura, R. A. R., Botelho, C. M. S. & Santos, S. C. R. 2017 Arsenic removal from water using iron-coated seaweeds. *Journal of Environmental Management* **192**, 224–233.

Wan, M. W., Petrisor, I. G., Lai, H. T., Kim, D. & Yen, T. F. 2004 Copper adsorption through chitosan immobilized on sand to demonstrate the feasibility for in situ soil decontamination. *Carbohydrate Polymers* **55** (3), 249–254.

Wan Ngah, W. S. & Fatinathan, S. 2008 Adsorption of Cu(II) ions in aqueous solution using chitosan beads, chitosan-GLA beads and chitosan alginate beads. *Chemical Engineering Journal* **143**, 62–72.

Weber Jr., W. J. & Morris, J. C. 1963 Kinetics of adsorption on carbon from solution. *Journal of the Sanitary Engineering Division, American Society of Civil Engineers* **89** (2), 31–60.

Wu, X. L., Wang, L., Chen, C. L., Xu, A. W. & Wang, X. K. 2011 Water-dispersible magnetite-graphene-LDH composites for efficient arsenate removal. *Journal of Materials Chemistry* **21** (43), 17353–17359.

Yoon, Y., Zheng, M., Ahn, Y. T., Park, W. K., Yang, W. S. & Kang, J. W. 2017 Synthesis of magnetite/non-oxidative graphene composites and their application for arsenic removal. *Separation and Purification Technology* **178**, 40–48.

Zhang, S., Zhou, Y., Nie, W., Song, L. & Zhang, T. 2012 Preparation of uniform magnetic chitosan microcapsules and their application in adsorbing copper ion(II) and chromium ion(III). *Industrial and Engineering Chemistry Research* **51**, 14099–14106.

Zhang, L., Hu, P., Wang, J. & Huang, R. 2016 Crosslinked quaternized chitosan/bentonite composite for the removal of Amino black 10B from aqueous solutions. *International Journal of Biological Macromolecules* **93**, 217–225.

First received 6 March 2018; accepted in revised form 19 July 2018. Available online 26 July 2018